

Geometric aspects of mixed quantum states inside the Bloch sphere

Paul M. Alsing¹, Carlo Cafaro^{2,3}, Domenico Felice^{3,4}, Orlando Luongo^{3,5,6,7,8}

¹*Air Force Research Laboratory, Information Directorate, 13441 Rome, New York, USA*

²*University at Albany-SUNY, Albany, NY 12222, USA*

³*SUNY Polytechnic Institute, Utica, NY 13502, USA*

⁴*Scuola Militare Nunziatella, Napoli 80132, Italy*

⁵*Università di Camerino, Camerino 62032, Italy*

⁶*INAF-Osservatorio Astronomico di Brera, Milano 20121, Italy*

⁷*INFN, Sezione di Perugia, Perugia 06123, Italy and*

⁸*Al-Farabi Kazakh National University, Almaty 050040, Kazakhstan*

When studying the geometry of quantum states, it is acknowledged that mixed states can be distinguished by infinitely many metrics. Unfortunately, this freedom causes metric-dependent interpretations of physically significant geometric quantities such as complexity and volume of quantum states. In this paper, we present an insightful discussion on the differences between the Bures and the Sjöqvist metrics inside a Bloch sphere. First, we begin with a formal comparative analysis between the two metrics by critically discussing three alternative interpretations for each metric. Second, we illustrate explicitly the distinct behaviors of the geodesic paths on each one of the two metric manifolds. Third, we compare the finite distances between an initial and final mixed state when calculated with the two metrics. Interestingly, in analogy to what happens when studying topological aspects of real Euclidean spaces equipped with distinct metric functions (for instance, the usual Euclidean metric and the taxicab metric), we observe that the relative ranking based on the concept of finite distance among mixed quantum states is not preserved when comparing distances determined with the Bures and the Sjöqvist metrics. Finally, we conclude with a brief discussion on the consequences of this violation of a metric-based relative ranking on the concept of complexity and volume of mixed quantum states.

PACS numbers: Quantum Computation (03.67.Lx), Quantum Information (03.67.Ac), Riemannian Geometry (02.40.Ky).

I. INTRODUCTION

It is established that there exist infinitely many distinguishability metrics for mixed quantum states [1]. For this reason, there is a certain degree of arbitrariness in selecting the metric when characterizing physical aspects of quantum states in mixed states. In particular, this freedom can cause metric-dependent explanations of geometric quantities with a clear physical significance, including complexity [2] and volume [3–6] of quantum states. Two examples of metrics for mixed quantum states are the Bures [7–10] and the Sjöqvist [11] metrics. In Ref. [12], we proposed a first explicit characterization of the Bures and Sjöqvist metrics over the manifolds of thermal states for specific spin qubit and superconducting flux qubit Hamiltonian models. We observed that while both metrics become the Fubini-Study metric in the asymptotic limiting case of the inverse temperature approaching infinity for both Hamiltonian models, the two metrics are generally distinct when far from the zero-temperature limit. The two metrics differ in the presence of a nonclassical behavior specified by the noncommutativity of neighboring mixed quantum states. Such a noncommutativity, in turn, is taken into account by the two metrics differently. As a follow up of our work in [12], we used the concept of decompositions of density operators by means of ensembles of pure quantum states to present in Ref. [13] an unabridged mathematical investigation on the relation between the Sjöqvist metric and the Bures metric for arbitrary nondegenerate mixed quantum states. Furthermore, to deepen our comprehension of the difference between these two metrics from a physics standpoint, we compared the general expressions of these two metrics for arbitrary thermal quantum states for quantum systems in equilibrium with a reservoir at non-zero temperature. Then, for clarity, we studied the difference between these two metrics in the case of a spin-qubit in an arbitrarily oriented uniform and stationary external magnetic field in thermal equilibrium with a finite-temperature bath. Finally, we showed in Ref [13] that the Sjöqvist metric does not satisfy the so-called monotonicity property [1], unlike the Bures metric. An interesting observable consequence, in terms of complexity behaviors, of this freedom in choosing between the Bures and Sjöqvist metrics was reported in Ref. [2]. There, devoting our attention to geodesic lengths and curvature properties for manifolds of mixed quantum states, we recorded a softening of the information geometric complexity [14, 15] on the Bures manifold compared to the Sjöqvist manifold.

In this paper, motivated by our findings in Refs. [2, 12, 13], we present a more in depth conceptual discussion on the differences between the Bures and the Sjöqvist metrics inside a Bloch sphere. To achieve this goal, we first begin by presenting in Section II a formal comparative analysis between the two metrics. This analysis is based upon a critical

Metric	Riemannian property	Monotonicity
Bures	Yes	Yes
Hilbert-Schmidt	Yes	No
Sjöqvist	Yes	No
Trace	No	Yes

TABLE I: Examples of metrics in the space of quantum states characterized in terms of Riemannian property and monotonicity.

discussion on three different alternative interpretations for each one of the two metrics. We then continue in Section III with an explicit illustration of the different behaviors of the geodesic paths on each one of the two metric manifolds. In the same section, we also compare the finite distances between an initial and final mixed state when calculated by means of the two metrics. Inspired by what happens when studying topological aspects of real Euclidean spaces equipped with distinct metric functions (for instance, the usual Euclidean metric and the taxicab metric), we observe in Section IV that the relative ranking based on the concept of finite distance among mixed quantum states is not preserved when comparing distances determined with the Bures and the Sjöqvist metrics. We then discuss in Section IV the consequences of this violation of a metric-based relative ranking on the concept of complexity and volume of mixed quantum states, along with other geometric peculiarities of the Bures and the Sjöqvist metrics inside a Bloch sphere. Our concluding remarks appear in Section V. Finally, for the ease of presentation, some more technical details appear in Appendix A and B.

II. LINE ELEMENTS

In this section, we begin with a presentation of a formal comparative analysis between the Bures and the Sjöqvist metrics inside a Bloch sphere. For completeness, we first mention in Table I some examples of metrics for mixed quantum states and characterize them in terms of their Riemannian and monotonicity properties. For more details on the notion of monotonicity and Riemannian property for quantum metrics, we refer to Ref. [1]. Returning to our main analysis, we focus here on the geometry of single-qubit mixed quantum states characterized by density operators on a two-dimensional Hilbert space. In this case, an arbitrary density operator ρ can be written as a decomposition of four-linear operators (i.e., four (2×2) -matrices) given by the identity operator I and the usual Pauli vector operator $\vec{\sigma} \stackrel{\text{def}}{=} (\sigma_x, \sigma_y, \sigma_z)$ [16]. Explicitly, we have

$$\rho \stackrel{\text{def}}{=} \frac{1}{2} (I + \vec{p} \cdot \vec{\sigma}), \quad (1)$$

where $\vec{p} \stackrel{\text{def}}{=} p\hat{p}$ denotes the three-dimensional Bloch vector. Note that p is the length $\|\vec{p}\| \stackrel{\text{def}}{=} \sqrt{\vec{p} \cdot \vec{p}}$ of the polarization vector \vec{p} , while \hat{p} is the unit vector. Following the vectors and one-forms notation along with the line of reasoning presented in Refs. [17–19], we can formally recast \vec{p} and $\vec{\sigma}$ in Eq. (1) as

$$\vec{p} \stackrel{\text{def}}{=} \sum_{i=1}^3 p^i \hat{e}_i, \text{ and } \vec{\sigma} \stackrel{\text{def}}{=} \sum_{i=1}^3 \sigma^i \hat{e}_i, \quad (2)$$

respectively. Observe that $\{\hat{e}_i\}_{1 \leq i \leq 3}$ is a set of orthonormal three-dimensional vectors satisfying $\hat{e}_i \cdot \hat{e}_j = \delta_{ij}$, with δ_{ij} being the Kronecker delta symbol. Moreover, we have $(\sigma^1, \sigma^2, \sigma^3) \stackrel{\text{def}}{=} (\sigma_x, \sigma_y, \sigma_z)$. For pure states, $\rho = \rho^2$, $\text{tr}(\rho) = \text{tr}(\rho^2) = 1$, and $p = 1$. Therefore, pure states are located on the surface of the unit two-sphere. For mixed states, instead, $\rho \neq \rho^2$, $\text{tr}(\rho) = 1$, and $\text{tr}(\rho^2) \leq 1$. Since $\text{tr}(\rho^2) = p^2$, we have $p \leq 1$. Therefore, mixed quantum states are located inside the unit two-sphere, i.e., they belong to the interior of the Bloch sphere.

In next two subsections, we study the geometric aspects of the interior of the Bloch sphere specified by the Bures and the Sjöqvist line elements, respectively.

A. The Bures line element

In the case of the Bures geometry, the infinitesimal line element $ds_{\text{Bures}}^2(\vec{p}, \vec{p} + d\vec{p})$ between two neighboring mixed states ρ and $\rho + d\rho$ corresponding to Bloch vectors \vec{p} and $\vec{p} + d\vec{p}$ is given by [9, 17, 18]

$$ds_{\text{Bures}}^2(\vec{p}, \vec{p} + d\vec{p}) = \frac{1}{4} \left[\frac{(\vec{p} \cdot d\vec{p})^2}{1 - p^2} + d\vec{p} \cdot d\vec{p} \right] = \frac{1}{4} \left[\frac{dp^2}{1 - p^2} + p^2(d\hat{p} \cdot d\hat{p}) \right]. \quad (3)$$

The equality between the first and second expressions of $ds_{\text{Bures}}^2(\vec{p}, \vec{p} + d\vec{p})$ in Eq. (3) can be checked by first noting that $\hat{p} \cdot \hat{p} = 1$ implies $\hat{p} \cdot d\hat{p} = 0$. This, in turn, yields the relations $d\vec{p} \cdot d\vec{p} = dp^2 + p^2 d\hat{p} \cdot d\hat{p}$ and $(\vec{p} \cdot d\vec{p})^2 = p^2 dp^2$. Finally, the use of these two identities allows us to arrive at the equality between the two expressions in Eq. (3).

1. First interpretation

We wish to critically discuss the structure of $ds_{\text{Bures}}^2(\vec{p}, \vec{p} + d\vec{p})$ in Eq. (3). To interpret the term $d\hat{p} \cdot d\hat{p}$ in $ds_{\text{Bures}}^2(\vec{p}, \vec{p} + d\vec{p})$, it is convenient to recast the polarization vector in spherical coordinates as $\vec{p} = (p^1, p^2, p^3) \stackrel{\text{def}}{=} (p \sin(\theta) \cos(\varphi), p \sin(\theta) \sin(\varphi), p \cos(\theta))$. Note that in spherical coordinates, we also have $(\hat{e}_1, \hat{e}_2, \hat{e}_3) = (\hat{e}_r, \hat{e}_\theta, \hat{e}_\varphi)$. It then follows that $d\vec{p} \cdot d\vec{p} = dp^2 + p^2(d\theta^2 + \sin^2(\theta) d\varphi^2)$ and $(\vec{p} \cdot d\vec{p})^2 = p^2 dp^2$. Finally, noting that the unit polarization vector is $\hat{p} = (\sin(\theta) \cos(\varphi), \sin(\theta) \sin(\varphi), \cos(\theta))$, we get after some algebra that $d\hat{p} \cdot d\hat{p} = d\theta^2 + \sin^2(\theta) d\varphi^2$. From this last relation, it clearly follows that $d\hat{p} \cdot d\hat{p}$ represents the usual line element $d\Omega^2 \stackrel{\text{def}}{=} d\theta^2 + \sin^2(\theta) d\varphi^2$ on a unit two-sphere. Therefore, when using spherical coordinates, the line element in Eq. (3) can be recast as

$$ds_{\text{Bures}}^2(\vec{p}, \vec{p} + d\vec{p}) = \frac{1}{4} \left[\frac{dp^2}{1 - p^2} + p^2(d\theta^2 + \sin^2(\theta) d\varphi^2) \right]. \quad (4)$$

From Eq. (3), it happens that when p is kept constant and equal to p_0 , a surface specified by the relation $p = p_0$ inside the Bloch sphere exhibits the geometry of a two-sphere of area $4\pi p_0^2$. As mentioned in Refs. [17, 18], the term $dp^2/(1 - p^2)$ in $ds_{\text{Bures}}^2(\vec{p}, \vec{p} + d\vec{p})$ implies that the inside of the Bloch sphere is not flat, but curved. Indeed, moving away from the origin of the sphere, the circumference $C(p) \stackrel{\text{def}}{=} 2\pi p$ of a circle of radius p on the two-sphere grows as $dC/ds \sim p' \stackrel{\text{def}}{=} dp/ds$ with s being the affine parameter. The distance $l(p) \stackrel{\text{def}}{=} \int_{s(0)}^{s(p)} p'/(1 - p^2)^{1/2} ds$ from the center, instead, grows as $dl/ds \sim p'/(1 - p^2)^{1/2} \geq p'$. Therefore, $l(p)$ grows at a faster rate than $C(p)$. This discrimination in growth rates for $C(p)$ and $l(p)$ signifies that the interior of the Bloch sphere is curved.

2. Second interpretation

A second useful coordinate system to further gain insights into the Bures line element in Eq. (3) is specified by considering a change of variables defined by $p \stackrel{\text{def}}{=} \sin(\chi)$ with χ being the hyperspherical angle with $0 \leq \chi \leq \pi/2$. In this set of coordinates, $4ds_{\text{Bures}}^2(\vec{p}, \vec{p} + d\vec{p})$ reduces to

$$4ds_{\text{Bures}}^2 = d\chi^2 + \sin^2(\chi) d\hat{p} \cdot d\hat{p}, \quad (5)$$

with $d\hat{p} \cdot d\hat{p} = d\Omega^2 \stackrel{\text{def}}{=} d\theta^2 + \sin^2(\theta) d\varphi^2$. Note that Eq. (5) for the Bures metric is exactly the (intrinsic) metric on the unit 3-sphere S^3 , where χ, θ , and φ are the angular coordinates on the sphere. For completeness, we remark that the metric for the $(N + 1)$ -sphere can be written in terms of the metric for the N -sphere, with the introduction of a new hyperspherical angle [1]. Two additional considerations are in order here. First, the four-dimensional vector $x^\mu(s) \equiv (x^0(s), \vec{x}(s))$ with $0 \leq \mu \leq 3$ such that $dx^\mu dx_\mu = 4ds_{\text{Bures}}^2 = d\chi^2 + \sin^2(\chi) d\hat{p} \cdot d\hat{p}$ can be written as $x^\mu(s) = x^0(s) \hat{e}_0(s) + \vec{x}(s)$. The quantity $x^0(s) \stackrel{\text{def}}{=} \chi(s)$ is the component of $x^\mu(s)$ along the direction $\hat{e}_0(s) \stackrel{\text{def}}{=} \vec{\chi}/\chi$, with $\hat{e}_0(s) \cdot \hat{e}_i(s) = 0$ for any $1 \leq i \leq 3$. The three-dimensional vector $\vec{x}(s)$ given by

$$\vec{x}(s) = \int \sin[\chi(s)] \frac{d\hat{p}(s)}{ds} ds, \quad (6)$$

specifies the remaining three coordinates of $x^\mu(s)$ along the directions $\hat{e}_1(s) \stackrel{\text{def}}{=} e_r(s)$, $\hat{e}_2(s) \stackrel{\text{def}}{=} e_\theta(s)$, and $\hat{e}_3(s) \stackrel{\text{def}}{=} e_\varphi(s)$. From Eq. (6) we point out the presence of a correlational structure between the motion along $\hat{e}_0(s)$ and the “spatial” directions $\hat{e}_i(s)$ with $1 \leq i \leq 3$. This correlational structure is a manifestation of the fact that for the Bures geometry, radial and angular motions inside the Bloch sphere are correlated since the dynamical geodesic equations are specified by a set of second order coupled nonlinear differential equations when using a set of spherical coordinates [2]. Second, remembering that line element in the usual cylindrical coordinates (ρ, φ, z) is $ds_{\text{cylinder}}^2 = dz^2 + d\Omega_{\text{cylinder}}^2$ where $d\Omega_{\text{cylinder}}^2 \stackrel{\text{def}}{=} d\rho^2 + \rho^2 d\varphi^2$, we observe that the structure of the Bures line element rewritten as in Eq. (5) is suggestive of the structure of a line element in the standard cylindrical coordinates once we make the connection between the pair $(\chi, d\Omega)$ with the pair $(\rho, d\Omega_{\text{cylinder}})$. Then, one can link a cylinder with a variable radius in the case of the Bures geometry. In particular, it is worth mentioning at this point that the non constant radius in the Bures case is upper bounded by the constant value that defines the radius in the Sjöqvist geometry (as we shall see in the next subsection). These geometric insights emerging from this simple change of coordinates would lead one to reasonably expect different lengths of geodesic paths in the two geometries studied here. This will be discussed in more detail in the next section, however.

3. Third interpretation

An alternative third set of coordinates for the Bures line element in Eq. (3) is given by the four coordinates x^μ with $0 \leq \mu \leq 3$ given by $x^\mu = (x^0, \vec{x}) \stackrel{\text{def}}{=} (\sqrt{1-p^2}, \vec{p})$ with $\vec{p} = p\hat{p}$. Indeed, from $x^0 = \sqrt{1-p^2}$, we get $(dx^0)^2 = (\vec{p} \cdot d\vec{p})^2 / (1-p^2)$. Therefore, when employing this coordinate system, the inside of the Bloch sphere can be described by a three-dimensional surface defined by the constraint relation $(x^0)^2 + \vec{x} \cdot \vec{x} = 1$. Moreover, the geometry of the surface is induced by the four-dimensional flat Euclidean line element [9],

$$4ds_{\text{Bures}}^2 = (dx^0)^2 + d\vec{x} \cdot d\vec{x}. \quad (7)$$

Notice that Eq. (7) for the Bures metric is the (extrinsic) metric on the unit 3-sphere S^3 viewed as embedded in \mathbb{R}^4 . The geodesic paths emerging from ds_{Bures}^2 in Eq. (7) are great circles on the 3-sphere. In terms of the arc length s , these geodesics can be recast as [17, 18]

$$x^\mu(s) = u^\mu \cos(s) + v^\mu \sin(s), \quad (8)$$

where $u^\mu = (u^0, \vec{u}) \stackrel{\text{def}}{=} (\cos(\chi), \hat{n} \sin(\chi))$, $v^\mu = (v^0, \vec{v}) \stackrel{\text{def}}{=} (\sin(\xi), \hat{m} \cos(\xi))$, $\hat{n} \cdot \hat{n} = \hat{m} \cdot \hat{m} = 1$, and $-(\hat{n} \cdot \hat{m}) \tan(\chi) = \tan(\xi)$. This last relation assures that $u^\mu \perp v^\mu$ so that Eq. (7) is satisfied for $x^\mu(s)$ given in Eq. (8).

We are now ready to critically discuss the Sjöqvist line element by mimicking the discussion performed for the Bures line element.

B. The Sjöqvist line element

In the case of the Sjöqvist geometry, the infinitesimal line element $ds_{\text{Sjöqvist}}^2(\vec{p}, \vec{p} + d\vec{p})$ between two neighboring mixed states ρ and $\rho + d\rho$ corresponding to Bloch vectors \vec{p} and $\vec{p} + d\vec{p}$ is given by [11]

$$ds_{\text{Sjöqvist}}^2(\vec{p}, \vec{p} + d\vec{p}) = \frac{1}{4} \left[\frac{2p^2 - 1}{p^4(1-p^2)} (\vec{p} \cdot d\vec{p})^2 + \frac{d\vec{p} \cdot d\vec{p}}{p^2} \right] = \frac{1}{4} \left[\frac{dp^2}{1-p^2} + (d\hat{p} \cdot d\hat{p}) \right]. \quad (9)$$

The equality between the first and second expressions of $ds_{\text{Sjöqvist}}^2(\vec{p}, \vec{p} + d\vec{p})$ in Eq. (9) can be verified by first observing that $\hat{p} \cdot \hat{p} = 1$ implies $\hat{p} \cdot d\hat{p} = 0$. This, in turn, leads to the relations $d\vec{p} \cdot d\vec{p} = dp^2 + p^2 d\hat{p} \cdot d\hat{p}$ and $(\vec{p} \cdot d\vec{p})^2 = p^2 dp^2$. Finally, exploiting these two relations, we arrive at the equality between the two expressions in Eq. (9).

We remark that Sjöqvist in Ref. [11] was the first to seek a deeper understanding of the physics behind the metric, with the concept of mixed state geometric phases playing a key role. However, for completeness, we also point out that what we call “Sjöqvist interferometric metric” first appeared as a special case of a more general family of metrics proposed in a more formal mathematical setting in Refs. [20, 21] by Andersson and Heydari. In this generalized setting, different metrics arise from different gauge theories, they are specified by distinct notions of horizontality and,

finally, they can be well-defined for both nondegenerate and degenerate mixed quantum states. Great part of the underlying gauge theory of this generalized family of metrics was developed in Ref. [22]. A suitable comprehensive reference to read about such generalized family of metrics is Chapter 5 in Andersson's thesis [23] where, in particular, the singular properties of Sjöqvist's metrics are discussed in Section 5.3.2. For further technical details on this matter, we refer to Ref. [23] and references therein.

1. First interpretation

We begin by noting that the term $dp^2/(1-p^2)$ in $ds_{\text{Sjöqvist}}^2(\vec{p}, \vec{p} + d\vec{p})$ implies that the inside of the Bloch sphere is not flat, but curved. In particular, the interpretation of this term follows exactly the discussion provided in the previous subsection for the Bures case. Moreover, similarly to the Bures case, the term $d\hat{p} \cdot d\hat{p}$ remains the standard line element $d\Omega^2 \stackrel{\text{def}}{=} d\theta^2 + \sin^2(\theta) d\varphi^2$ on a unit two-sphere. Therefore, when using spherical coordinates, the line element in Eq. (9) can be recast as

$$ds_{\text{Sjöqvist}}^2(\vec{p}, \vec{p} + d\vec{p}) = \frac{1}{4} \left[\frac{dp^2}{1-p^2} + d\theta^2 + \sin^2(\theta) d\varphi^2 \right]. \quad (10)$$

Unlike what happens in the Bures case, when p is kept constant and equal to p_0 , a surface specified by the relation $p = p_0$ inside the Bloch sphere exhibits the geometry of a two-sphere of area 4π in the Sjöqvist case. The area 4π of this two-sphere is greater than the area $4\pi p_0^2$ that specifies the Bures case and, in addition, does not depend on the choice of the constant value p_0 of p . This is a signature of the fact that, in the Sjöqvist case, the accessible regions inside the Bloch sphere have volumes greater than those specifying the Bures geometry. Indeed, this observation was first pointed out in Ref. [2] and shall be further discussed in the forthcoming interpretations.

2. Second interpretation

In analogy to the second interpretation proposed for the Bures metric, a convenient coordinate system to further gain insights into the Sjöqvist line element in Eq. (9) can be achieved by performing a change of variables defined by $p \stackrel{\text{def}}{=} \sin(\chi)$ with χ being the hyperspherical angle with $0 \leq \chi \leq \pi/2$. In this set of coordinates, $4ds_{\text{Sjöqvist}}^2(\vec{p}, \vec{p} + d\vec{p})$ reduces to

$$4ds_{\text{Sjöqvist}}^2(\vec{p}, \vec{p} + d\vec{p}) = d\chi^2 + d\hat{p} \cdot d\hat{p}, \quad (11)$$

with $d\hat{p} \cdot d\hat{p} = d\Omega^2 \stackrel{\text{def}}{=} d\theta^2 + \sin^2(\theta) d\varphi^2$. Observe that Eq. (11) for the Sjöqvist metric exhibits a structure that is similar to that of the metric on $S^1 \times S^2$, the Cartesian product of the unit 1-sphere S^1 with the unit 2-sphere S^2 . This Cartesian product is responsible for the uncorrelated structure between the hyperspherical angle coordinate and the pair of angular coordinates (θ, φ) (i.e., the polar and azimuthal angles, respectively). This uncorrelated structure, in turn, manifests itself with an expression of the metric on $S^1 \times S^2$ which is simply the sum of the metrics on S^1 and S^2 . More specifically, comparing Eqs. (5) and (11), we note that in the Sjöqvist case, unlike the Bures case, the “temporal” and “spatial” spatial components of the metric are no longer correlated. In particular, the analogue of $\vec{x}(s)$ in Eq. (6) reduces to

$$\vec{x}(s) = \int \frac{d\hat{p}(s)}{ds} ds. \quad (12)$$

From Eq. (12) we emphasize the absence of a correlational structure between the motion along $\hat{e}_0(s)$ and the “spatial” directions $\hat{e}_i(s)$ with $1 \leq i \leq 3$. Interestingly, the lack of this correlational structure manifests itself when using spherical coordinates to describe the Sjöqvist geometry. Specifically, it emerges from the fact that the radial and angular motions inside the Bloch sphere are not correlated since the dynamical geodesic equations are specified by a set of second order uncoupled nonlinear differential equations [2]. Lastly, recalling that line element in the usual cylindrical coordinates (ρ, φ, z) is $ds_{\text{cylinder}}^2 = dz^2 + d\Omega_{\text{cylinder}}^2$ where $d\Omega_{\text{cylinder}}^2 \stackrel{\text{def}}{=} d\rho^2 + \rho^2 d\varphi^2$, we note that the structure of the Sjöqvist line element recast as in Eq. (11) is reminiscent of the structure of a line element in the traditional cylindrical coordinates once we connect the pair $(\chi, d\Omega)$ with the pair $(\rho, d\Omega_{\text{cylinder}})$. Then, unlike what happens in the Bures case, one can associate a cylinder with a constant value of its radius in the case of the Sjöqvist geometry. In particular, the constant value of the radius upper bounds any value that the varying radius can assume in the Bures case. Again, as previously mentioned, these geometric insights that arise from this simple change of

coordinates would lead one to expect different lengths of geodesic paths in the two geometries studied here. However, this will be studied in more detail in the next section. In what follows, instead, we present our third and last interpretation.

3. Third interpretation

Following the third interpretation presented for the Bures case, we adapt the four coordinates x^μ with $0 \leq \mu \leq 3$ given by $x^\mu = (x^0, \vec{x}) \stackrel{\text{def}}{=} (\sqrt{1-p^2}, \vec{p})$ with $\vec{p} = p\hat{p}$ to the Sjöqvist line element $ds_{\text{Sjöqvist}}^2(\vec{p}, \vec{p} + d\vec{p})$ in Eq. (9). After some algebra, we get

$$4ds_{\text{Sjöqvist}}^2 = \omega_{x^0}(p) (dx^0)^2 + \omega_{\vec{x}}(p) d\vec{x} \cdot d\vec{x}, \quad (13)$$

with $\omega_{x^0}(p) \stackrel{\text{def}}{=} (2p^2 - 1)/p^4$ and $\omega_{\vec{x}}(p) \stackrel{\text{def}}{=} 1/p^2$. Note that Eq. (13) for the Sjöqvist metric is the (extrinsic) metric for $S^1 \times S^2$ embedded in \mathbb{R}^4 . The embedding of $S^1 \times S^2$ in \mathbb{R}^4 appears to be more complicated than that of S^3 in \mathbb{R}^4 . This complication, in turn, leads to a behavior of the Sjöqvist metric which is more irregular than that observed in the Bures case. More specifically, comparing Eqs. (7) and (13), we note that unlike what happens in the Bures case, the inside of the Bloch sphere is no longer a unit 3-sphere embedded in a four-dimensional flat Euclidean space with geodesics given by great circles on it when using the four coordinates x^μ . In particular, the metric $4ds_{\text{Sjöqvist}}^2$ as expressed in Eq. (13) is not regular since its signature is not constant. Indeed, $\omega_{x^0}(p) \geq 0$ for $p \geq 1/\sqrt{2}$ and $\omega_{x^0}(p) \leq 0$ for $0 \leq p \leq 1/\sqrt{2}$. An essential singularity appears at $p = 0$ (i.e., for maximally mixed states). This observation, although obtained from a different perspective, is in agreement with what was originally noticed in Ref. [11]. Finally, the geodesic paths change as well. Indeed, the geodesics $[x^\mu(s)]_{\text{Bures}} \stackrel{\text{def}}{=} [x^0(s), \vec{x}(s)]$ in Eq. (7) are formally replaced by $[x^\mu(s)]_{\text{Sjöqvist}}$ expressed in terms of $[x^0(s)]_{\text{Sjöqvist}}$ and $[\vec{x}(s)]_{\text{Sjöqvist}}$ as

$$[x^0(s)]_{\text{Bures}} \rightarrow [x^0(s)]_{\text{Sjöqvist}} \stackrel{\text{def}}{=} \int \sqrt{|\omega_{x^0}(p)|} \frac{dx^0(s)}{ds} ds, \quad (14)$$

and

$$[\vec{x}(s)]_{\text{Bures}} \rightarrow [\vec{x}(s)]_{\text{Sjöqvist}} \stackrel{\text{def}}{=} \int \frac{1}{\sqrt{\omega_{\vec{x}}(p)}} \frac{d\vec{x}(s)}{ds} ds, \quad (15)$$

respectively. For completeness and following the terminology of the previous subsection, we point out that $p(s)$ in Eqs. (14) and (15) equals $p(s) \stackrel{\text{def}}{=} \left\{ 1 - [\cos(\chi) \cos(s) + \sin(\xi) \sin(s)]^2 \right\}^{1/2}$ and is such that $0 \leq p(s) \leq 1$.

In this section, we focused our attention on grasping physical insights from the infinitesimal line elements for the Bures and the Sjöqvist metrics inside a Bloch sphere in Eqs. (3) and (9), respectively. In the next section, we shall further explore some of our insights by extending our focus to the difference between the finite distances of geodesic paths connecting mixed quantum states on these two metric manifolds.

III. FINITE DISTANCES

In this section, we turn our attention to the study of the behaviors of the geodesic paths on each one of the two metric manifolds, i.e. Bures and Sjöqvist manifolds. Furthermore, we also offer a comparison between the finite distances between arbitrary initial and final mixed states when calculated by means of the above mentioned metrics. For clarity, we remark that to compare finite distances between mixed quantum states in the Bloch ball calculated with the Bures and Sjöqvist metrics, it is sufficient to focus on points in the xz -plane. This is a consequence of two facts. First, distances are preserved under rotations. Second, it is possible to construct a suitable composition of two $\text{SO}(3; \mathbb{R})$ rotations acting on arbitrary Bloch vectors for mixed states, say \vec{p}_1 and \vec{p}_2 , such that the distances $\mathcal{L}(\vec{p}_1, \vec{p}_2) = \mathcal{L}(\vec{p}_{1,\text{new}}, \vec{p}_{2,\text{new}})$ with $\vec{p}_{1,\text{new}}$ and $\vec{p}_{2,\text{new}}$ belonging to the xz -plane. For further details, we refer to Appendix A.

A. The Bures distance

We begin by using spherical coordinates (r, θ, φ) and keep $\varphi = \text{const.}$ Then, geodesics are obtained by minimizing $\int ds_{\text{Bures}}$ over all curves connecting points (r_a, θ_a) and (r_b, θ_b) . More specifically, one arrives at the curve $[\theta_a, \theta_b] \ni$

$\theta \mapsto r_{\text{Bures}}(\theta) \in [0, 1]$ that minimizes the length $\mathcal{L}_{\text{Bures}}(\vec{a}, \vec{b})$ defined as

$$\mathcal{L}_{\text{Bures}}(\vec{a}, \vec{b}) \stackrel{\text{def}}{=} \int_{s_a}^{s_b} \sqrt{ds_{\text{Bures}}^2} = \frac{1}{2} \int_{\theta_a}^{\theta_b} L(r', r, \theta) d\theta, \quad (16)$$

with ds_{Bures}^2 in Eq. (4). In Eq. (16), $r' \stackrel{\text{def}}{=} dr/d\theta$ and $L(r', r, \theta)$ is the Lagrangian-like function defined as

$$L(r', r, \theta) \stackrel{\text{def}}{=} \sqrt{r^2 + \frac{r'^2}{1-r^2}}. \quad (17)$$

From Eq. (36), note that $L = L(r', r)$ in Eq. (17) does not explicitly depend θ . Therefore, $\partial L / \partial \theta = 0$. In this case, it happens that the Euler-Lagrange equation

$$\frac{d}{d\theta} \frac{\partial L(r', r)}{\partial r'} - \frac{\partial L(r', r)}{\partial r} = 0, \quad (18)$$

reduces to the well-known Beltrami identity in Lagrangian mechanics,

$$L(r', r) - r' \frac{\partial L(r', r)}{\partial r'} = \text{const.} \quad (19)$$

Indeed, making use of Eq. (18) together with the identity

$$\frac{dL(r', r)}{d\theta} = \frac{\partial L(r', r)}{\partial r'} r'' + \frac{\partial L(r', r)}{\partial r} r', \quad (20)$$

we get

$$\frac{dL(r', r)}{d\theta} = \frac{d}{d\theta} \left(r' \frac{\partial L(r', r)}{\partial r'} \right). \quad (21)$$

Finally, Eq. (21) leads to the so-called Beltrami identity in Eq. (19). Using Eqs. (17) and (19), we obtain

$$\frac{r^2}{\sqrt{r^2 + \frac{r'^2}{1-r^2}}} = \text{const.} \equiv c_B. \quad (22)$$

Manipulating Eq. (22) and imposing the boundary conditions $r(\theta_a) = r_a$ and $r(\theta_b) = r_b$, we obtain

$$\int_{r_a}^{r_b} \frac{dr}{\sqrt{r^2 \left(\frac{r^2}{c_B^2} - 1 \right) (1-r^2)}} = \int_{\theta_a}^{\theta_b} d\theta, \quad (23)$$

with $0 < c_B \leq r \leq 1$. For notational simplicity, let us set $a_B^2 \stackrel{\text{def}}{=} 1/c_B^2 > 1$. Then, integration of Eq. (23) by use of Mathematica yields

$$I(r) \stackrel{\text{def}}{=} \int \frac{dr}{\sqrt{r^2 \left(\frac{r^2}{c_B^2} - 1 \right) (1-r^2)}} = \frac{r\sqrt{r^2-1}\sqrt{a_B^2 r^2-1}}{\sqrt{-r^2(r^2-1)(a_B^2 r^2-1)}} \tanh^{-1} \left(\frac{\sqrt{r^2-1}}{\sqrt{a_B^2 r^2-1}} \right) + \text{const.} \quad (24)$$

Manipulating Eq. (24), $I(r)$ in Eq. (24) becomes

$$I(r) = -\arctan \left(\frac{\sqrt{1-r^2}}{\sqrt{a_B^2 r^2-1}} \right) + \text{const.} \quad (25)$$

Finally, substituting Eq. (25) into Eq. (23), the radial geodesic path in the Bures case can be recast as [2]

$$r_{\text{Bures}}(\theta) = \sqrt{\frac{1 + \tan^2 [\mathcal{A}_B(r_a, r'_a) - (\theta - \theta_a)]}{1 + a_B^2 (r_a, r'_a) \tan^2 [\mathcal{A}_B(r_a, r'_a) - (\theta - \theta_a)]}}, \quad (26)$$

where the constants $\mathcal{A}_B(r_a, r'_a)$ and $a_B^2(r_a, r'_a)$ in Eq. (26) are given by

$$\mathcal{A}_B(r_a, r'_a) \stackrel{\text{def}}{=} \arctan \left(\sqrt{(1-r_a^2)^2 \left(\frac{r_a}{r'_a}\right)^2} \right), \text{ and } a_B^2(r_a, r'_a) \stackrel{\text{def}}{=} \frac{1}{r_a^2} + \left(\frac{r'_a}{r_a}\right)^2 \frac{1}{r_a^2(1-r_a^2)}, \quad (27)$$

respectively. At this point, we recall that the Bures distance between two density operators ρ_1 and ρ_2 is given by [9],

$$\mathcal{L}_{\text{Bures}}(\rho_1, \rho_2) \stackrel{\text{def}}{=} \sqrt{2} \left[1 - \text{tr} \left(\sqrt{\sqrt{\rho_1} \rho_2 \sqrt{\rho_1}} \right) \right]^{1/2}. \quad (28)$$

Furthermore, $\mathcal{L}_{\text{Bures}}(\rho_1, \rho_2)$ in Eq. (28) can be expressed in terms of the fidelity between two density operators ρ_1 and ρ_2 defined as [24, 25]

$$F(\rho_1, \rho_2) \stackrel{\text{def}}{=} \left(\text{tr} \left(\sqrt{\sqrt{\rho_1} \rho_2 \sqrt{\rho_1}} \right) \right)^2. \quad (29)$$

Therefore, combining Eqs. (28) and (29), the Bures distance $\mathcal{L}_{\text{Bures}}(\rho_1, \rho_2)$ becomes

$$\mathcal{L}_{\text{Bures}}(\rho_1, \rho_2) = \sqrt{2} \left[1 - \sqrt{F(\rho_1, \rho_2)} \right]^{1/2}. \quad (30)$$

Then, focusing on qubit states, the fidelity $F(\rho_1, \rho_2)$ in Eq. (29) reduces to [24]

$$F(\rho_1, \rho_2) = \text{tr}(\rho_1 \rho_2) + 2\sqrt{\det(\rho_1) \det(\rho_2)}, \quad (31)$$

where ρ_1 and ρ_2 are given by

$$\rho_1 = \rho(\vec{a}) \stackrel{\text{def}}{=} \frac{\mathbf{I} + \vec{a} \cdot \vec{\sigma}}{2}, \text{ and } \rho_2 = \rho(\vec{b}) \stackrel{\text{def}}{=} \frac{\mathbf{I} + \vec{b} \cdot \vec{\sigma}}{2}, \quad (32)$$

respectively. Using Eqs. (32) and (31), $\mathcal{L}_{\text{Bures}}(\rho_1, \rho_2)$ in Eq. (30) reduces to

$$\mathcal{L}_{\text{Bures}}(\rho_1, \rho_2) = \sqrt{2} \left[1 - \sqrt{2 \left(\frac{1 + \vec{a} \cdot \vec{b}}{4} + \sqrt{\frac{1 - \vec{a}^2}{4} \frac{1 - \vec{b}^2}{4}} \right)} \right]^{1/2}. \quad (33)$$

For Bloch vectors $\vec{a} \stackrel{\text{def}}{=} r_a \hat{n}_a$ and $\vec{b} \stackrel{\text{def}}{=} r_b \hat{n}_b$ in the xz -plane, we have $\hat{n}_a \stackrel{\text{def}}{=} (\sin(\theta_a), 0, \cos(\theta_a))$ and $\hat{n}_b \stackrel{\text{def}}{=} (\sin(\theta_b), 0, \cos(\theta_b))$ with θ_a and θ_b in $[0, \pi]$. Therefore, in this scenario, $\mathcal{L}_{\text{Bures}}(\rho_1, \rho_2) = \mathcal{L}_{\text{Bures}}(\rho_1(\vec{a}), \rho_2(\vec{b})) = \mathcal{L}_{\text{Bures}}(\vec{a}, \vec{b})$ in Eq. (33) is equal to

$$\mathcal{L}_{\text{Bures}}(\vec{a}, \vec{b}) = \sqrt{2} \left[1 - \sqrt{2 \left(\frac{1 + r_a r_b \cos(\theta_a - \theta_b)}{4} + \sqrt{\frac{1 - r_a^2}{4} \frac{1 - r_b^2}{4}} \right)} \right]^{1/2}. \quad (34)$$

The expression of $\mathcal{L}_{\text{Bures}}(\vec{a}, \vec{b})$ in Eq. (34) helps us evaluating the finite distance between arbitrary mixed states $\rho(\vec{a}) \stackrel{\text{def}}{=} (\mathbf{I} + \vec{a} \cdot \vec{\sigma})/2$ and $\rho(\vec{b}) \stackrel{\text{def}}{=} (\mathbf{I} + \vec{b} \cdot \vec{\sigma})/2$ belonging to the xz -plane and, thus, for arbitrary states in the Bloch ball (for details, see Appendix A).

B. The Sjöqvist distance

Following Sjöqvist's work in Ref. [11], we focus on finding geodesic paths that connect points (i.e., mixed quantum states) in the Bloch ball that lay in a plane that contains the origin. Employing spherical coordinates (r, θ, φ) and maintaining $\varphi = \text{const.}$, geodesics can be obtained by minimizing $\int ds_{\text{Sjöqvist}}$ over all curves connecting points $\vec{a} \leftrightarrow (r_a, \theta_a)$ and $\vec{b} \leftrightarrow (r_b, \theta_b)$. More specifically, we aim to get the curve $[\theta_a, \theta_b] \ni \theta \mapsto r_{\text{Sjöqvist}}(\theta) \in (0, 1]$ that minimizes the length $\mathcal{L}_{\text{Sjöqvist}}(\vec{a}, \vec{b})$ given by

$$\mathcal{L}_{\text{Sjöqvist}}(\vec{a}, \vec{b}) \stackrel{\text{def}}{=} \int_{s_a}^{s_b} \sqrt{ds_{\text{Sjöqvist}}^2} = \frac{1}{2} \int_{\theta_a}^{\theta_b} L(r', r, \theta) d\theta, \quad (35)$$

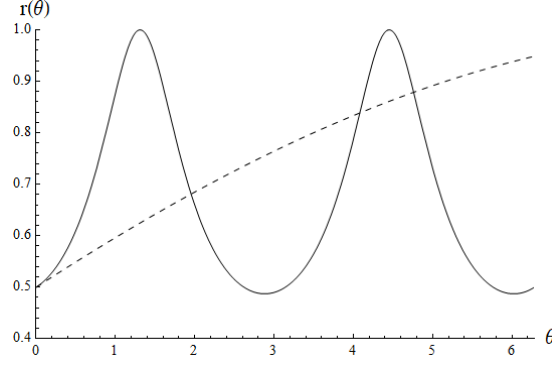


FIG. 1: Illustrative depiction of Bures and Sjöqvist curves $r_{\text{Bures}}(\theta)$ (solid line) and $r_{\text{Sjöqvist}}(\theta)$ (dashed line), respectively, for identical boundary conditions specified by the initial position ($r(\theta_a) = r_a \stackrel{\text{def}}{=} 1/2$) and the initial speed ($r'(\theta_a) = r'_a \stackrel{\text{def}}{=} 0.1$). Note that $\theta_a \leq \theta \leq \theta_b$, with $\theta_a \stackrel{\text{def}}{=} 0$ and $\theta_b \stackrel{\text{def}}{=} 2\pi$.

with $ds_{\text{Sjöqvist}}^2$ in Eq. (10). In Eq. (35), $r' \stackrel{\text{def}}{=} dr/d\theta$ and $L(r', r, \theta)$ is the Lagrangian-like function defined as

$$L(r', r, \theta) \stackrel{\text{def}}{=} \sqrt{1 + \frac{r'^2}{1 - r^2}}. \quad (36)$$

Following the similar derivation of the Euler-Lagrange equations leading to Eq. (22) in the previous subsection for the Bures metric, we obtain

$$\frac{1}{\sqrt{1 + \frac{r'^2}{1 - r^2}}} = \text{const.} \equiv c_S, \quad (37)$$

that is,

$$\frac{r'^2}{1 - r^2} = \text{const.} \equiv k \stackrel{\text{def}}{=} \frac{1 - c_S^2}{c_S^2}, \quad (38)$$

Integrating Eq. (38) and imposing the boundary conditions $r(\theta_a) = r_a$, $r(\theta_b) = r_b$, with $\theta_{\text{initial}} = \theta_a$ and $\theta_{\text{final}} = \theta_b$, we obtain the geodesic path

$$r_{\text{Sjöqvist}}(\theta) = \sin \left\{ \frac{\sin^{-1}(r_b) - \sin^{-1}(r_a)}{\theta_b - \theta_a} \theta + \frac{\sin^{-1}(r_a) + \sin^{-1}(r_b)}{2} - \frac{1}{2} \frac{\theta_a + \theta_b}{\theta_b - \theta_a} [\sin^{-1}(r_b) - \sin^{-1}(r_a)] \right\}. \quad (39)$$

We remark that the expression of $r_{\text{Sjöqvist}}(\theta)$ in Eq. (39) can be recast, alternatively, in terms of boundary conditions on the initial position $r(\theta_a) = r_a$ and the initial speed $r'(\theta_a) = r'_a$. We get, after some algebra [2],

$$r_{\text{Sjöqvist}}(\theta) = \sin \left[\frac{r'_a}{\sqrt{1 - r_a^2}} (\theta - \theta_a) + \sin^{-1}(r_a) \right]. \quad (40)$$

As a consistency check, we observe that we correctly recover Eq. (18) in Ref. [11] when we set $\theta_{\text{initial}} = 0$ in Eq. (39). For illustrative purposes, we present in Fig. 1 a plot of the Bures and Sjöqvist curves $r_{\text{Bures}}(\theta)$ in Eq. (26) and $r_{\text{Sjöqvist}}(\theta)$ in Eq. (40), respectively, for identical boundary conditions specified by the initial position and the initial speed. Finally, inserting $r_{\text{Sjöqvist}}(\theta)$ in Eq. (39) into the expression for $L(r', r, \theta)$ in Eq. (36), $\mathcal{L}_{\text{Sjöqvist}}(\vec{a}, \vec{b})$ in Eq. (35) reduces to [11]

$$\mathcal{L}_{\text{Sjöqvist}}(\vec{a}, \vec{b}) = \frac{1}{2} \sqrt{(\theta_b - \theta_a)^2 + [\sin^{-1}(r_b) - \sin^{-1}(r_a)]^2}. \quad (41)$$

The expression of $\mathcal{L}_{\text{Sjöqvist}}(\vec{a}, \vec{b})$ in Eq. (41) allows us to calculate the finite distance between arbitrary mixed states $\rho(\vec{a}) \stackrel{\text{def}}{=} (\mathbf{I} + \vec{a} \cdot \vec{\sigma})/2$ and $\rho(\vec{b}) \stackrel{\text{def}}{=} (\mathbf{I} + \vec{b} \cdot \vec{\sigma})/2$ laying in the xz -plane and, thus, for arbitrary states in the Bloch ball (for details, see Appendix A). For illustrative purposes, we plot in part (a) of Fig. 2 the Sjöqvist distance $\mathcal{L}_{\text{Sjöqvist}}(\Delta\theta)$

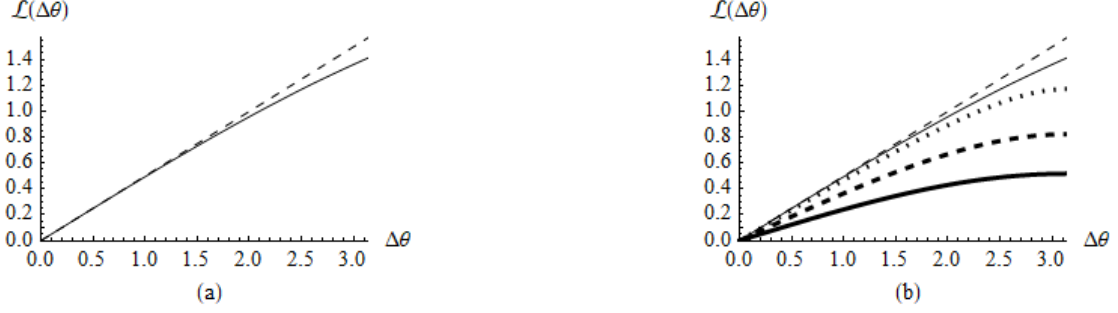


FIG. 2: In (a), we plot the Sjöqvist distance $\mathcal{L}_{\text{Sjöqvist}}(\Delta\theta)$ (dashed line) and the Bures distance $\mathcal{L}_{\text{Bures}}(\Delta\theta)$ (solid line) versus $\Delta\theta \stackrel{\text{def}}{=} \theta_b - \theta_a$ with $0 \leq \Delta\theta \leq \pi$ in the assumption that $r_a = r_b = 1$. In (b), we compare the Sjöqvist and Bures distances as in (a) but for different values of $r_a = r_b = \text{const.}$ with $\text{const.} \in \{1, 0.95, 0.75, 0.5\}$. While the Sjöqvist distance (thin dashed line) does not depend on the particular value of the const., the Bures distance depends on the specific value of the const. (thin solid line for $r = 1$, thick dotted line for $r = 0.95$, thick dashed line for $r = 0.75$, and thick solid line for $r = 0.5$). In any case, we have $0 \leq \mathcal{L}_{\text{Bures}}(\Delta\theta) \leq \mathcal{L}_{\text{Sjöqvist}}(\Delta\theta) \leq \pi/2 \approx 1.57$.

in Eq. (41) and the Bures distance $\mathcal{L}_{\text{Bures}}(\Delta\theta)$ in Eq. (34) versus $\Delta\theta \stackrel{\text{def}}{=} \theta_b - \theta_a$ with $0 \leq \Delta\theta \leq \pi$ in the assumption that $r_a = r_b = 1$. In part (b) of Fig. 2, instead, we compare the Sjöqvist and Bures distances as in (a) but for different values of $r_a = r_b = \text{const.}$ with $\text{const.} \in \{1, 0.95, 0.75, 0.5\}$. We observe that while the Sjöqvist distance does not depend on the particular value of the const., the Bures distance depends on the specific value of the const. In any case, we have $0 \leq \mathcal{L}_{\text{Bures}}(\Delta\theta) \leq \mathcal{L}_{\text{Sjöqvist}}(\Delta\theta) \leq \pi/2$. For completeness, we recall that the geodesic distance between two orthogonal pure states represented by antipodal points on the Bloch sphere is π , whereas the corresponding Fubini-Study distance is $\pi/2$. In the limit of $r_a = r_b = 1$, the Bures distance in Eq. (34) reduces to the Fubini-Study distance $|\Delta\theta|/2$ with $\Delta\theta \stackrel{\text{def}}{=} \theta_b - \theta_a$ only approximately since $\mathcal{L}_{\text{Bures}}(\Delta\theta) = |\Delta\theta|/2 + O(|\Delta\theta|^3)$ when $|\Delta\theta| \ll 1$. In the same limiting case of $r_a = r_b = 1$, instead, the Sjöqvist distance in Eq. (41) reduces to the Fubini-Study distance $|\Delta\theta|/2$ in an exact manner.

Thanks to Eqs. (34) and (41), we are now ready to provide some intriguing discussion points in the next section.

IV. DISCUSSION

In this section, we briefly comment on some peculiar geometric features that emerge from the Bures and Sjöqvist finite distances in Eqs. (34) and (41) obtained in Section III. To make our discussion closer to classical geometric and topological arguments, we carry out a comparative discussion highlighting formal similarities between the classical (Euclidean, Taxicab) metrics in the xz -plane of \mathbb{R}^2 and the quantum (Bures, Sjöqvist) metrics inside the Bloch sphere. Let us denote with d_{Euclid} and d_{Taxicab} the usual Euclidean and Taxicab metric functions, respectively. For completeness, we recall that $d_{\text{Euclid}}(\vec{a}, \vec{b}) \stackrel{\text{def}}{=} \sqrt{(a_x - b_x)^2 + (a_z - b_z)^2}$ and $d_{\text{Taxicab}}(\vec{a}, \vec{b}) \stackrel{\text{def}}{=} |a_x - b_x| + |a_z - b_z|$ with $\vec{a} \stackrel{\text{def}}{=} (a_x, a_z)$, $\vec{b} \stackrel{\text{def}}{=} (b_x, b_z)$ in \mathbb{R}^2 . First, we observe that although $(\mathbb{R}^2, d_{\text{Euclid}})$ and $(\mathbb{R}^2, d_{\text{Taxicab}})$ are topologically equivalent metric spaces [26], we have that $d_{\text{Euclid}}(P_i, P_{i'}) \leq d_{\text{Euclid}}(P_k, P_{k'})$ does not imply that $d_{\text{Taxicab}}(P_i, P_{i'}) \leq d_{\text{Taxicab}}(P_k, P_{k'})$ with $i \neq i'$ and $k \neq k'$. Therefore, a relative ranking of pairs of points specified in terms of distances between the pairs themselves, with closer pairs of points ranking higher than those further away, is not preserved when using Euclidean and Taxicab metrics. For instance, consider a set \mathcal{S}_1 of three points in \mathbb{R}^2 given in Cartesian coordinates by $\mathcal{S}_1 \stackrel{\text{def}}{=} \left\{ P_1 \stackrel{\text{def}}{=} (0, 0), P_2 \stackrel{\text{def}}{=} (0, 1), P_3 \stackrel{\text{def}}{=} ((1 + \sqrt{2})/4, (1 + \sqrt{2})/4) \right\}$. One notices that $d_{\text{Euclid}}(P_1, P_2) = 1 \geq 0.85 \simeq d_{\text{Euclid}}(P_1, P_3)$. However, when using the Taxicab metric, we have $d_{\text{Taxicab}}(P_1, P_2) = 1 \leq 1.21 \simeq d_{\text{Taxicab}}(P_1, P_3)$. Interestingly, the conservation of this type of ranking of pairs of points is violated also when comparing the Bures and Sjöqvist metrics. For instance, consider a set \mathcal{S}_2 of four points (i.e., mixed quantum states) $P_i \leftrightarrow \rho(P_i) = (I + \vec{a}_i \cdot \vec{\sigma})/2$ with \vec{a}_i assumed to belong to the xz -plane and specified by the pair of spherical coordinates (r_{a_i}, θ_{a_i}) given by $\mathcal{S}_2 \stackrel{\text{def}}{=} \left\{ P_1 \stackrel{\text{def}}{=} (1/2, 0), P_2 \stackrel{\text{def}}{=} (1/2, \pi), P_3 \stackrel{\text{def}}{=} (1/8, 0), P_4 \stackrel{\text{def}}{=} (1/4, \pi) \right\}$. Then, in terms of the Bures metric, we find $d_{\text{Bures}}(P_1, P_2) \simeq 0.52 \geq 0.19 \simeq d_{\text{Bures}}(P_3, P_4)$. However, when using the Sjöqvist metric, we get $d_{\text{Sjöqvist}}(P_1, P_2) = \pi/2 \simeq 1.570 \leq 1.572 \simeq d_{\text{Sjöqvist}}(P_3, P_4)$. Clearly, $d_{\text{Bures}}(P_i, P_j) = d_{\text{Bures}}(\vec{a}_i, \vec{a}_j) = \mathcal{L}_{\text{Bures}}(\vec{a}_i, \vec{a}_j)$ as defined in Eq. (34). Similarly, $d_{\text{Sjöqvist}}(P_i, P_j) = d_{\text{Sjöqvist}}(\vec{a}_i, \vec{a}_j) = \mathcal{L}_{\text{Sjöqvist}}(\vec{a}_i, \vec{a}_j)$ as defined

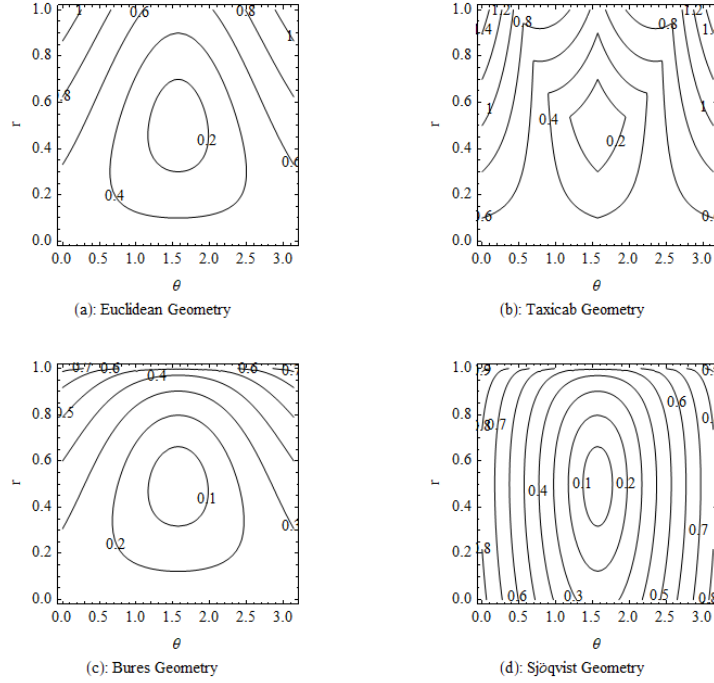


FIG. 3: In (a), we illustrate the Euclidean geometry in terms of a contour plot that exhibits the spherical coordinates r v.s. θ with $0 \leq r \leq 1$ and $0 \leq \theta \leq \pi$. The level curves are given by $\mathcal{L}_{\text{Euclid}}(\vec{a}, \vec{b}) = c$, with c being a positive constant, $\vec{a} \stackrel{\text{def}}{=} (r_a \cos(\theta_a), r_a \sin(\theta_a)) = (0, 1/2)$ with $(r_a, \theta_a) \stackrel{\text{def}}{=} (1/2, \pi/2)$, and $\vec{b} \stackrel{\text{def}}{=} (r \cos(\theta), r \sin(\theta))$. In (b), we follow (a) and depict the Taxicab geometry with level curves specified by the relation $\mathcal{L}_{\text{Taxicab}}(\vec{a}, \vec{b}) = c$. In (c), we illustrate the Bures geometry in terms of the contour plot that shows the spherical coordinates r v.s. θ with $0 \leq r \leq 1$ and $0 \leq \theta \leq \pi$. The level curves are characterized by the relation $\mathcal{L}_{\text{Bures}}(\vec{a}, \vec{b}) = c$, with c being a positive constant. The vectors \vec{a} and \vec{b} are as in (a) and (b). Finally, following (c), we depict in (d) the Sjöqvist geometry with level curves defined by $\mathcal{L}_{\text{Sjöqvist}}(\vec{a}, \vec{b}) = c$. Again, the vectors \vec{a} and \vec{b} are as in (a), (b), and (c). Finally, the expressions for $\mathcal{L}_{\text{Euclid}}(\vec{a}, \vec{b})$, $\mathcal{L}_{\text{Taxicab}}(\vec{a}, \vec{b})$, $\mathcal{L}_{\text{Bures}}(\vec{a}, \vec{b})$, and $\mathcal{L}_{\text{Sjöqvist}}(\vec{a}, \vec{b})$ are the ones that appear in the main text.

in Eq. (41). We also emphasize here that unlike what happens in the Bures geometry, in the Sjöqvist geometry it is possible to identify pairs of two points, say $(P_i, P_{i'})$ and $(P_k, P_{k'})$, that seem to be visually rankable which, in actuality, are at the same distance from each other (and, thus, non-rankable according to our previously mentioned notion of relative ranking). For example, following the terminology introduced for the set \mathcal{S}_2 , consider the new set of points \mathcal{S}_3 defined as $\mathcal{S}_3 \stackrel{\text{def}}{=} \{P_1 \stackrel{\text{def}}{=} (1/4, 0), P_2 \stackrel{\text{def}}{=} (1/4, \pi), P_3 \stackrel{\text{def}}{=} (1/2, 0), P_4 \stackrel{\text{def}}{=} (1/2, \pi)\}$. Then, when employing the Sjöqvist metric, we find $d_{\text{Sjöqvist}}(P_1, P_2) = d_{\text{Sjöqvist}}(P_3, P_4) = \pi/2$, even though the pair of points (P_3, P_4) seem to be visually more distant than the pair of points (P_1, P_2) . However, when employing the Bures metric, we get $d_{\text{Bures}}(P_1, P_2) \simeq 0.25 \leq 0.52 \simeq d_{\text{Bures}}(P_3, P_4)$. This latter inequality is consistent with our visual intuition associated with seeing these points as mixed states inside the Bloch sphere. Clearly, these different geometric features between Bures and Sjöqvist geometries can be ascribed to the formal structure of the expressions for the finite distances in Eqs. (34) and (41), respectively, that we have obtained in the previous section. Second, in addition to the fact that $d_{\text{Euclid}}(P_i, P_j) \leq d_{\text{Taxicab}}(P_i, P_j) \leftrightarrow d_{\text{Bures}}(P_i, P_j) \leq d_{\text{Sjöqvist}}(P_i, P_j)$, it can be noted that a given probe point in the Sjöqvist manifold appears to be locally surrounded by a greater number of points at the same distance from the source. This, in turn, can be regarded as an indicator of the presence of a higher degree of complexity during the change from an initial point (source state) to a final point (target state). Therefore, this set of points of discussion that we are offering here seem to land additional support to the apparent emergence of a softer degree of complexity in Bures manifolds when compared with Sjöqvist manifolds [2]. For completeness, we point out that once we find a single violation of either the former (classical) or the latter (quantum) inequalities, we can find several sets of points that would yield the same violation. From a classical geometry standpoint, this is a consequence of the fact that distances are invariant under isometries. In particular, limiting our discussion to the case at hand, any planar isometry mapping input points in \mathbb{R}^2 to output points in \mathbb{R}^2 is either a pure translation, a pure rotation about some center, or a reflection followed by a translation (i.e., a glide reflection). Moreover, the composition of two isometries is an isometry. From a quantum standpoint, instead, an isometry is an inner-product preserving transformation

that maps, in general, between Hilbert spaces with different dimensions. In the particular scenario in which input and output Hilbert spaces have the same dimensions, the isometry is simply a unitary operation. For a general discussion on the role of isometries in quantum information and computation, we refer to Refs. [27, 28]. Finally, for an illustrative visualization of the Euclidean, Taxicab, Bures, and Sjöqvist geometries that summarizes most of our discussion points, we refer to Fig. 3. Interestingly, inspired by the expression of the Bures fidelity $F_{\text{Bures}}(\vec{a}, \vec{b}) = \left[1 - \mathcal{L}_{\text{Bures}}^2(\vec{a}, \vec{b}) / (\mathcal{L}_{\text{Bures}}^2)_{\text{max}}\right]^2$ with $(\mathcal{L}_{\text{Bures}})_{\text{max}} = \sqrt{2}$, one may think of considering a sort of Sjöqvist fidelity given by $F_{\text{Sjöqvist}}(\vec{a}, \vec{b}) = \left[1 - \mathcal{L}_{\text{Sjöqvist}}^2(\vec{a}, \vec{b}) / (\mathcal{L}_{\text{Sjöqvist}}^2)_{\text{max}}\right]^2$ with $(\mathcal{L}_{\text{Sjöqvist}})_{\text{max}} = \pi/2$. From these fidelities, define the ratio $\mathcal{R}(\vec{a}, \vec{b}) \stackrel{\text{def}}{=} F_{\text{Sjöqvist}}(\vec{a}, \vec{b}) / F_{\text{Bures}}(\vec{a}, \vec{b})$ with \vec{a}, \vec{b} as in Fig. 3 (for example). Then, one can check that the area of the two-dimensional parametric region with parameters r and θ and specified by the conditions $0 \leq \mathcal{R}(\vec{a}, \vec{b}) \leq 1$, i.e. the region where Bures fidelity is larger than the Sjöqvist fidelity, is greater than 50% of the total accessible two-dimensional parametric region with area given by π (i.e., the Lebesgue measure $\mu_{\text{Lebesgue}}([0, 1]_r \times [0, \pi]_\theta)$ of the interval $[0, 1]_r \times [0, \pi]_\theta$). Therefore, this type of approximate reasoning can be viewed as a semi-quantitative indication of the higher degree of distinguishability of mixed quantum states by means of the Bures metric. Clearly, a deeper comprehension of these facts would require an analysis extended to arbitrary initial parametric configurations along with a more rigorously defined version of $\mathcal{R}(\vec{a}, \vec{b})$. Nevertheless, we believe that interesting insights emerge from our approximate semi-quantitative discussion proposed here. We are now ready for our conclusions.

V. FINAL REMARKS

In this paper, building on our recent works in Refs. [2, 12, 13], we presented more comprehensive discussion on the differences between the Bures and the Sjöqvist metrics inside a Bloch sphere. First, inspired by the works by Caves and Braunstein in Refs. [17, 18], we offered a formal comparative analysis between the two metrics by critically discussing three alternative interpretations for each metric. For the Bures metric, the three interpretations appear in Eqs. (4), (5), and (7). For the Sjöqvist metric, instead, the corresponding three interpretations emerge from Eqs. (10), (11), and (13), respectively. Second, we illustrated (Fig. 1) in an explicit fashion the different behaviors of the geodesic paths (Eqs. (26) and (40) for the Bures and Sjöqvist metrics cases, respectively) on each one of the two metric manifolds. Third, we compared (Fig. 2) the finite distances between an initial and final mixed state when calculated with the two metrics (Eqs. (34) and (41) for the Bures and Sjöqvist metrics cases, respectively). Thanks to Eqs. (34) and (41) for $\mathcal{L}_{\text{Bures}}(\vec{a}, \vec{b})$ and $\mathcal{L}_{\text{Sjöqvist}}(\vec{a}, \vec{b})$, respectively, we were able to provide some intriguing discussion points (along with a visual aid coming from Fig. 3) concerning some similarities between classical (Euclidean, Taxicab) metrics in \mathbb{R}^2 and quantum (Bures, Sjöqvist) metrics inside the Bloch sphere. In particular, we argued that the fact that the Sjöqvist metric yields longer finite distances, denser clouds of states that are equidistant from a fixed source state and, finally, an unnatural violation of distance-based relative ranking of pairs of points inside the Bloch sphere is at the origin of the higher degree of complexity of the Sjöqvist manifold compared with the Bures manifold as reported in Ref. [2].

In the usual three-dimensional physical space, we ordinarily state that the reason why it is difficult to distinguish two points is because they are close together. In classical and quantum geometry, one tends to invert this line of reasoning and claim that two points on a statistical manifold must be very close together because it is hard to differentiate them [29]. In particular, within the geometry of mixed quantum states, increasing distance seems to correspond to more reliable distinguishability [10]. From Figs. 3(c) and 3(d), we note that for a given accessible region $I_r \times I_\theta \stackrel{\text{def}}{=} [0, 1] \times [0, \pi]$ the lower density of level curves in the Bures case is consistent with the observed softening of the complexity of motion on Bures manifolds compared with Sjöqvist manifolds [2]. Indeed, considering points at the same distance from the source state as indistinguishable and viewing indistinguishability as an obstruction to the evolution to new distinguishable states to be traversed before arriving at a possible target state, a lower degree of the complexity of motion would correspond to an accessible region made up of a greater number of discernible states. Loosely speaking, Sjöqvist manifolds have some sort of “*quantum labyrinth*” structure greater than the one corresponding to Bures manifolds. Therefore, one can risk to encounter longer paths of indistinguishability and, thus, can necessitate to explore larger accessible regions before landing to the sought target state [2, 30–32].

In this work, we focused on geometric aspects of two specific metrics for mixed quantum states. For a general discussion on the relevant criteria an arbitrary quantum distance must satisfy in order to be both experimentally and theoretically meaningful, we refer to Refs. [33, 34]. In particular, for a discussion on how to experimentally determine the Bures and Sjöqvist distances by means of interferometric procedures, we refer to Refs. [35] and [11, 36], respectively. Moreover, we emphasize that our work here does not consider the role of space-time geometry, as the quantum metrics we discuss are purely Riemannian. However, given some formal similarities between the quantum

Bures and the classical closed Robertson-Walker spatial geometries (Appendix B), it would be interesting to begin from this formal link and elaborate on it so to help shedding some light on how to construct suitable versions of quantum space-time geometries that can incorporate relativistic physical effects within the framework of quantum physics [37–41].

In summary, despite its limitations, we hope our work will motivate other researchers and pave the way to additional investigations on the interplay between quantum mechanics, geometry, and topological arguments. From our standpoint, we have strong reasons to believe this work will undoubtedly constitute a solid starting point for an extension of our recent work in Ref. [42] on qubit geodesics on the Bloch sphere from optimal-speed Hamiltonian evolutions to qubit geodesics inside the Bloch sphere. For the time being, we leave a more in-depth quantitative discussion on these potential geometric extensions of our analytical findings, including generalizations to mixed state geometry and quantum evolutions in higher-dimensional Hilbert spaces, to forthcoming scientific investigations.

Acknowledgments

P.M.A. acknowledges support from the Air Force Office of Scientific Research (AFOSR). C.C. thanks N. Andrzejewicz, B. Glindmyer, E. Liriano, and C. Neal for helpful discussions on Euclidean and Taxicab geometries. C.C. is also grateful to the United States Air Force Research Laboratory (AFRL) Summer Faculty Fellowship Program for providing support for this work. Any opinions, findings and conclusions or recommendations expressed in this material are those of the author(s) and do not necessarily reflect the views of the Air Force Research Laboratory (AFRL). The work of O.L. is partially financed by the Ministry of Higher Education and Science of the Republic of Kazakhstan, Grant: IRN AP19680128. Finally, O.L. is grateful to the Department of Physics of the Al-Farabi University for hospitality during the period in which the idea of this manuscript was discussed.

-
- [1] I. Bengtsson and K. Życzkowski, *Geometry of Quantum States*, Cambridge University Press (2006).
 - [2] C. Cafaro and P. M. Alsing, *Complexity of pure and mixed qubit geodesic paths on curved manifolds*, Phys. Rev. **D106**, 096004 (2022).
 - [3] K. Życzkowski, P. Horodecki, A. Sanpera, and M. Lewenstein, *Volume of the set of separable states*, Phys. Rev. **A58**, 883 (1998).
 - [4] K. Życzkowski, *Volume of the set of separable states. II*, Phys. Rev. **A60**, 3496 (1999).
 - [5] D. Felice, H. Q. Minh, and S. Mancini, *The volume of Gaussian states by information geometry*, J. Math. Phys. **58**, 012201 (2017).
 - [6] M. Rexiti, D. Felice, and S. Mancini, *The volume of two-qubit states by information geometry*, Entropy **20**, 146 (2018).
 - [7] D. Bures, *An extension of Kakutani's theorem on infinite product measures to the tensor product of semifinite ω^* -algebras*, Trans. Amer. Math. Soc. **135**, 199 (1969).
 - [8] A. Uhlmann, *The “transition probability” in the state space of a $*$ -algebra*, Rep. Math. Phys. **9**, 273 (1976).
 - [9] M. Hübner, *Explicit computation of the Bures distance for density matrices*, Phys. Lett. **A163**, 239 (1992).
 - [10] S. L. Braunstein and C. M. Caves, *Statistical distance and the geometry of quantum states*, Phys. Rev. Lett. **72**, 3439 (1994).
 - [11] E. Sjöqvist, *Geometry along evolution of mixed quantum states*, Phys. Rev. Research **2**, 013344 (2020).
 - [12] C. Cafaro and P. M. Alsing, *Bures and Sjöqvist metrics over thermal state manifolds for spin qubits and superconducting flux qubits*, Eur. Phys. J. Plus **138**, 655 (2023).
 - [13] P. M. Alsing, C. Cafaro, O. Luongo, C. Lupo, S. Mancini, and H. Quevedo, *Comparing metrics for mixed quantum states: Sjöqvist and Bures*, Phys. Rev. **A107**, 052411 (2023).
 - [14] C. Cafaro and S. A. Ali, *Jacobi fields on statistical manifolds of negative curvature*, Physica **D234**, 70 (2007).
 - [15] C. Cafaro, *The Information Geometry of Chaos*, PhD Thesis, State University of New York at Albany, Albany-NY, USA (2008).
 - [16] M. A. Nielsen and I. L. Chuang, *Quantum Computation and Quantum Information*, Cambridge University Press (2000).
 - [17] S. L. Braunstein and C. M. Caves, *Geometry of quantum states*, Annals of the New York Academy of Sciences **755**, 786 (1995).
 - [18] S. L. Braunstein and C. M. Caves, *Geometry of quantum states*. In: B. V. Belavkin, O. Hirota, and R. L. Hudson (Eds.), Quantum Communications and Measurement, pp 21-30. Springer, Boston, MA (1995).
 - [19] C. Cafaro and S. Mancini, *Characterizing the depolarizing quantum channel in terms of Riemannian geometry*, Int. J. Geom. Meth. Mod. Phys. **9**, 1260020 (2012).
 - [20] O. Andersson and H. Heydari, *Geometric uncertainty relation for mixed quantum states*, J. Math. Phys. **55**, 042110 (2014).
 - [21] O. Andersson and H. Heydari, *Quantum speed limits and optimal Hamiltonians for driven systems in mixed states*, J. Phys. A: Math. Theor. **47**, 215301 (2014).

- [22] O. Andersson and H. Heydari, *A symmetry approach to geometric phase for quantum ensembles*, J. Phys. A: Math. Theor. **48**, 485302 (2015).
- [23] O. Andersson, *Holonomy in Quantum Information Geometry*, Thesis for the degree of Licentiate of Philosophy in Theoretical Physics, arXiv:quant-ph/1910.08140 (2019).
- [24] R. Jozsa, *Fidelity for mixed quantum states*, Journal of Modern Optics **41**, 2315 (1994).
- [25] M. Wilde, *Quantum Information Theory*, Cambridge University Press (2017).
- [26] F. H. Croom, *Principles of Topology*, Dover Publications, Garden City, New York (2016).
- [27] L. Molnar and W. Timmermann, *Isometries of quantum states*, J. Phys. A: Math. Gen. **36**, 267 (2003).
- [28] R. Iten, R. Colbeck, I. Kukuljan, J. Home, and M. Christandl, *Quantum circuit for isometries*, Phys. Rev. **A93**, 032318 (2016).
- [29] A. Caticha, *Entropic Inference and the Foundations of Physics*, University of São Paulo Press, Brazil (2012).
- [30] C. Cafaro and S. Mancini, *Quantifying the complexity of geodesic paths on curved statistical manifolds through information geometric entropies and Jacobi fields*, Physica **D240**, 607 (2011).
- [31] S. A. Ali and C. Cafaro, *Theoretical investigations of an information geometric approach to complexity*, Rev. Math. Phys. **29**, 1730002 (2017).
- [32] C. Cafaro and S. A. Ali, *Information geometric measures of complexity with applications to classical and quantum physical settings*, Foundations **1**, 45 (2021).
- [33] A. Gilchrist, N. K. Langford, and M. A. Nielsen, *Distance measures to compare real and ideal quantum processes*, Phys. Rev. **A71**, 062310 (2005).
- [34] P. E. M. F. Mendonca, R. d. J. Napolitano, M. A. Marchioli, C. J. Foster, and Y.-C. Liang, *Alternative fidelity measure between quantum states*, Phys. Rev. **A78**, 052330 (2008).
- [35] K. Bartkiewicz, V. Travnicsek, and K. Lemr, *Measuring distances in Hilbert space by many-particle interference*, Phys. Rev. **A99**, 032336 (2019).
- [36] H. Silva, B. Mera, and N. Paunkovic, *Interferometric geometry from symmetry-broken Uhlmann gauge group with applications to topological phase transitions*, Phys. Rev. **B103**, 085127 (2021).
- [37] A. Peres and D. R. Terno, *Quantum information and relativity theory*, Rev. Mod. Phys. **76**, 93 (2004).
- [38] A. Peres, *Quantum information and general relativity*, Fortsch. Phys. **52**, 1052 (2004).
- [39] R. B. Mann and T. C. Ralph, *Relativistic quantum information*, Focus issue: Relativistic quantum information, Class. Quantum Grav. **29**, 220301 (2012).
- [40] P. M. Alsing and I. Fuentes, *Observer dependent entanglement*, Focus issue: Relativistic quantum information, Class. Quantum Grav. **29**, 224001 (2012).
- [41] P. M. Alsing, J. P. Dowling, and G. J. Milburn, *Ion trap simulations of quantum fields in an expanding Universe*, Phys. Rev. Lett. **94**, 220401 (2005).
- [42] C. Cafaro and P. M. Alsing, *Qubit geodesics on the Bloch sphere from optimal-speed Hamiltonian evolutions*, Class. Quantum Grav. **40**, 115005 (2023).
- [43] J. J. Sakurai, *Modern Quantum Mechanics*, Addison Wesley Publishing Company, Inc. (1985).
- [44] S. Weinberg, *Gravitation and Cosmology: Principles and Applications of the General Theory of Relativity*, John Wiley and Sons, Inc. (1972).
- [45] W. K. Wootters, *Statistical distance and Hilbert space*, Phys. Rev. **D23**, 357 (1981).
- [46] A. Aviles, C. Gruber, O. Luongo, and H. Quevedo, *Cosmography and constraints on the equation of state of the Universe in various parametrizations*, Phys. Rev. **D86**, 123516 (2012).
- [47] P. K. S. Dunsby and O. Luongo, *On the theory and applications of modern cosmography*, Int. J. Geom. Meth. Mod. Phys. **13**, 1630002 (2016).
- [48] C. W. Misner, K. S. Thorne, and J. A. Wheeler, *Gravitation*, W. H. Freeman & Company (1973).
- [49] H. O. Ohanian and R. Ruffini, *Gravitation and Spacetime*, W. W. Norton & Company (1976).
- [50] E. Newman and J. N. Goldberg, *Measurement of distance in general relativity*, Phys. Rev. **114**, 1391 (1959).
- [51] H.-J. Schmidt, *How should we measure spatial distances?*, Gen. Rel. Grav. **28**, 899 (1996).
- [52] F. De Felice and D. Bini, *Classical measurements in curved spacetime*, Cambridge University Press (2010).
- [53] C. MacLaurin, *Clarifying spatial distance measurement*, Proceedings of the Fifteenth Marcel Grossman Meeting, pp. 1372-1377 (2022).

Appendix A: Rotation of Bloch vectors

In this Appendix, we discuss some technical details needed to understand the reason why to compare finite distances between mixed quantum states in the Bloch ball calculated with the Bures and Sjöqvist metrics, it is sufficient to focus solely on points in the xz -plane. As mentioned in Section III, this is essentially due to two facts. First, one needs to recall that distances are preserved under rotations. Second, given two mixed states $\rho_1 = \rho(\vec{p}_1) \stackrel{\text{def}}{=} (\mathbf{I} + \vec{p}_1 \cdot \vec{\sigma})/2$ and $\rho_2 = \rho(\vec{p}_2) \stackrel{\text{def}}{=} (\mathbf{I} + \vec{p}_2 \cdot \vec{\sigma})/2$, one needs to exploit the fact that it is possible to construct a suitable composition of two $\text{SO}(3; \mathbb{R})$ rotations acting on arbitrary Bloch vectors for mixed states, say \vec{p}_1 and \vec{p}_2 , such that the distances $\mathcal{L}(\vec{p}_1, \vec{p}_2) = \mathcal{L}(\vec{p}_{1,\text{new}}, \vec{p}_{2,\text{new}})$ with $\vec{p}_{1,\text{new}}$ and $\vec{p}_{2,\text{new}}$ belonging to the xz -plane. In this Appendix, we wish to explicitly present these two $\text{SO}(3; \mathbb{R})$ rotations needed to accomplish this task.

In general, recall that the unitary evolution of the state $\rho(0)$ under the unitary evolution operator $U(t)$ can be described by $\rho(t) = U(t)\rho(0)U^\dagger(t)$. In terms of the Bloch vectors $\vec{a}(0)$ and $\vec{a}(t)$ with $\rho(0) \stackrel{\text{def}}{=} [\mathbf{I} + \vec{a}(0) \cdot \vec{\sigma}]/2$ and $\rho(t) \stackrel{\text{def}}{=} [\mathbf{I} + \vec{a}(t) \cdot \vec{\sigma}]/2$, respectively, we have that $\vec{a}(0)$ evolves to $\vec{a}(t)$ by following the transformation law $\vec{a}(t) = \mathcal{R}_{\hat{n}}(\alpha)\vec{a}(0)$. The quantity $\mathcal{R}_{\hat{n}}(\alpha)$ is an $\text{SO}(3; \mathbb{R})$ rotation about the \hat{n} -axis by an angle α . In general, the temporal dependence can be encoded into both \hat{n} and α . The relation between the $\text{SU}(2; \mathbb{C})$ counterclockwise rotation by the angle α about the axis \hat{n} , $U(\alpha, \hat{n}) = e^{-i\frac{\alpha}{2}\hat{n} \cdot \vec{\sigma}}$, and the $\text{SO}(3; \mathbb{R})$ rotation $\mathcal{R}_{\hat{n}}(\alpha)$ is given by [43],

$$[\mathcal{R}_{\hat{n}}(\alpha)]_{ij} \stackrel{\text{def}}{=} \frac{1}{2} \text{tr} [\sigma_i U(\alpha, \hat{n}) \sigma_j U^\dagger(\alpha, \hat{n})], \quad (\text{A1})$$

with $1 \leq i, j \leq 3$. In particular, using the explicit expression of $U(\alpha, \hat{n})$ [43]

$$U(\alpha, \hat{n}) = e^{-i\frac{\alpha}{2}\hat{n} \cdot \vec{\sigma}} = \begin{pmatrix} \cos(\frac{\alpha}{2}) - i \sin(\frac{\alpha}{2}) n_z & -i \sin(\frac{\alpha}{2}) (n_x - i n_y) \\ -i \sin(\frac{\alpha}{2}) (n_x + i n_y) & \cos(\frac{\alpha}{2}) + i \sin(\frac{\alpha}{2}) n_z \end{pmatrix}, \quad (\text{A2})$$

the (3×3) -rotation matrix $\mathcal{R}_{\hat{n}}(\alpha)$ in Eq. (A2) becomes

$$\mathcal{R}_{\hat{n}}(\alpha) = \begin{pmatrix} \cos(\alpha) + n_x^2 [1 - \cos(\alpha)] & n_x n_y [1 - \cos(\alpha)] - n_z \sin(\alpha) & n_x n_z [1 - \cos(\alpha)] + n_y \sin(\alpha) \\ n_y n_x [1 - \cos(\alpha)] + n_z \sin(\alpha) & \cos(\alpha) + n_y^2 [1 - \cos(\alpha)] & n_y n_z [1 - \cos(\alpha)] - n_x \sin(\alpha) \\ n_z n_x [1 - \cos(\alpha)] - n_y \sin(\alpha) & n_z n_y [1 - \cos(\alpha)] + n_x \sin(\alpha) & \cos(\alpha) + n_z^2 [1 - \cos(\alpha)] \end{pmatrix}. \quad (\text{A3})$$

To show that $\text{dist}(\rho_1, \rho_2) = \text{dist}(\rho_{1,\text{new}}, \rho_{2,\text{new}}) \leftrightarrow \text{dist}(\vec{p}_1, \vec{p}_2) = \text{dist}(\vec{p}_{1,\text{new}}, \vec{p}_{2,\text{new}})$, we need to make explicit the sequential action of the two $\text{SO}(3; \mathbb{R})$ rotation matrices that need to act simultaneously on the pair (\vec{p}_1, \vec{p}_2) . This will be described in two steps. In the first step, we transition from the arbitrary pair (\vec{p}_1, \vec{p}_2) with $\vec{p}_1 \stackrel{\text{def}}{=} (r_1 \sin(\theta_1) \cos(\varphi_1), r_1 \sin(\theta_1) \sin(\varphi_1), r_1 \cos(\theta_1))$ and $\vec{p}_2 \stackrel{\text{def}}{=} (r_2 \sin(\theta_2) \cos(\varphi_2), r_2 \sin(\theta_2) \sin(\varphi_2), r_2 \cos(\theta_2))$, respectively, to the new pair (\vec{p}'_1, \vec{p}'_2) given by

$$\vec{p}'_1 = \mathcal{R}_{\frac{\vec{p}_1 \times \hat{z}}{\|\vec{p}_1 \times \hat{z}\|}}(\theta_1) \vec{p}_1, \text{ and } \vec{p}'_2 = \mathcal{R}_{\frac{\vec{p}_1 \times \hat{z}}{\|\vec{p}_1 \times \hat{z}\|}}(\theta_1) \vec{p}_2, \quad (\text{A4})$$

respectively. In Eq. (A4), we have $\vec{p}'_1 = r_1 \hat{z}$, $\vec{p}'_2 = (r_2 \sin(\theta'_2) \cos(\varphi'_2), r_2 \sin(\theta'_2) \sin(\varphi'_2), r_2 \cos(\theta'_2))$, and the $\text{SO}(3; \mathbb{R})$ rotation matrix $\mathcal{R}_{\frac{\vec{p}_1 \times \hat{z}}{\|\vec{p}_1 \times \hat{z}\|}}(\theta_1)$ given by

$$\mathcal{R}_{\frac{\vec{p}_1 \times \hat{z}}{\|\vec{p}_1 \times \hat{z}\|}}(\theta_1) \stackrel{\text{def}}{=} \begin{pmatrix} \cos(\theta_1) + \sin^2(\varphi_1)(1 - \cos(\theta_1)) & -\sin(\varphi_1) \cos(\varphi_1)(1 - \cos(\theta_1)) & -\cos(\varphi_1) \sin(\theta_1) \\ -\sin(\varphi_1) \cos(\varphi_1)(1 - \cos(\theta_1)) & \cos(\theta_1) + \cos^2(\varphi_1)(1 - \cos(\theta_1)) & -\sin(\varphi_1) \sin(\theta_1) \\ \cos(\varphi_1) \sin(\theta_1) & \sin(\varphi_1) \sin(\theta_1) & \cos(\theta_1) \end{pmatrix}. \quad (\text{A5})$$

In the second step, we transition from the pair (\vec{p}'_1, \vec{p}'_2) to the final pair $(\vec{p}_{1,\text{new}}, \vec{p}_{2,\text{new}})$ given by

$$\vec{p}_{1,\text{new}} = \mathcal{R}_{\hat{z}}(\varphi'_2) \vec{p}'_1, \text{ and } \vec{p}_{2,\text{new}} = \mathcal{R}_{\hat{z}}(\varphi'_2) \vec{p}'_2, \quad (\text{A6})$$

respectively. In Eq. (A6), we have $\vec{p}_{1,\text{new}} = \vec{p}'_1 = r_1 \hat{z}$, $\vec{p}_{2,\text{new}} = (r_2 \sin(\theta'_2), 0, \cos(\theta'_2))$, and the $\text{SO}(3; \mathbb{R})$ rotation matrix $\mathcal{R}_{\hat{z}}(\varphi'_2)$ defined as

$$\mathcal{R}_{\hat{z}}(\varphi'_2) \stackrel{\text{def}}{=} \begin{pmatrix} \cos(\varphi'_2) & \sin(\varphi'_2) & 0 \\ -\sin(\varphi'_2) & \cos(\varphi'_2) & 0 \\ 0 & 0 & 1 \end{pmatrix}. \quad (\text{A7})$$

Clearly, before ending our discussion, we need to specify how to obtain the angles θ'_2 and φ'_2 . This can be easily accomplished thanks to our knowledge of the Bloch vector $\vec{p}_2 = (\vec{p}_2 \cdot \hat{x}, \vec{p}_2 \cdot \hat{y}, \vec{p}_2 \cdot \hat{z})$. More explicitly, the angles θ'_2 and φ'_2 are given by

$$\theta'_2 \stackrel{\text{def}}{=} \arccos \left(\frac{\vec{p}_2 \cdot \hat{z}}{\|\vec{p}_2\|} \right), \text{ and } \varphi'_2 \stackrel{\text{def}}{=} \frac{\vec{p}_2 \cdot \hat{y}}{|\vec{p}_2 \cdot \hat{y}|} \arccos \left(\frac{\vec{p}_2 \cdot \hat{x}}{\sqrt{(\vec{p}_2 \cdot \hat{x})^2 + (\vec{p}_2 \cdot \hat{y})^2}} \right), \quad (\text{A8})$$

respectively. Note that when $\vec{p}_2 \cdot \hat{x} > 0$, φ'_2 in Eq. (A8) reduces to $\arctan [(\vec{p}_2 \cdot \hat{y}) / (\vec{p}_2 \cdot \hat{x})]$. Thanks to the relations in Eq. (A8), our discussion can be considered complete now.

Appendix B: Bures geometry and closed Robertson-Walker spatial geometry

In this Appendix, we discuss some similarities between the quantum Bures and the classical closed Robertson-Walker spatial geometries. It is known that geodesic paths encode relevant information about the curved space being characterized by a proper metric. In general relativity, for instance, geodesic paths extend the concept of straight lines to curved space-time. In the geometry of quantum evolutions, instead, a geodesic is viewed as a path of minimal statistical length that connects two quantum states along which the maximal number of statistically distinguishable states is minimum. In Einstein's general theory of relativity, the dynamical evolution of a physical system is linked to the space-time geometry in a very neat manner. Specifically, space-time explains matter how to move. Matter, in turn, informs space-time how to curve. This link between matter and geometry is neatly summarized in Einstein's field equations [44], $[(8\pi G/c^4) \mathcal{T}_{\mu\nu}]_{\text{matter}} = [\mathcal{R}_{\mu\nu} - (1/2)g_{\mu\nu}\mathcal{R}]_{\text{geometry}}$. In the previous relation, G is Newton's gravitational constant, c is the speed of light in vacuum, $\mathcal{T}_{\mu\nu}$ is the stress-energy tensor, $\mathcal{R}_{\mu\nu}$ is the Ricci curvature tensor, \mathcal{R} is the scalar curvature, and, finally, $g_{\mu\nu}$ is the space-time metric tensor. In geometric formulations of quantum mechanics, the geometry on the space of quantum states, either pure [45] or mixed [10], specifies limitations on our capacity of discriminating one state from another by means of measurements. Therefore, unlike what happens in classical general relativity, the geometry on the space of quantum states does not express, in general, the actual dynamical evolution of a quantum system [17, 18].

Despite these differences, we remark that the Bures line element can be recast as (neglecting the constant multiplicative factor $1/4$)

$$ds_{\text{Bures}}^2 = d\chi^2 + \sin^2(\chi) [d\theta^2 + \sin^2(\theta) d\varphi^2], \quad (\text{B1})$$

and is identical to the spatial metric component of the (closed) spherical Robertson-Walker space-time metric that characterizes the so-called Freedman model in cosmology. This space-time metric is given by [44],

$$ds_{\text{RW}}^2 = -c^2 dt^2 + R^2(t) \left\{ \frac{dr^2}{1 - kr^2} + r^2 [d\theta^2 + \sin^2(\theta) d\varphi^2] \right\}, \quad (\text{B2})$$

where $R(t)$ is the cosmic scale factor and k the spatial curvature that can assume values $+1$ (spherical, or closed Universe), 0 (flat Universe), or -1 (hyperbolic, or open Universe). The dynamics of the space-time geometry, once k is fixed, is fully determined once the time-dependence of the cosmic scale factor is known [46, 47]. Setting $t = t_0$, $R(t_0) = 1$, and $k = 1$, Eq. (B2) reduced to the spatial metric

$$dl_{\text{RW}}^2 = \frac{dr^2}{1 - r^2} + r^2 [d\theta^2 + \sin^2(\theta) d\varphi^2]. \quad (\text{B3})$$

Then, performing a transformation from Cartesian to (spherical) polar coordinates given by $x \stackrel{\text{def}}{=} \sin(\chi) \sin(\theta) \cos(\varphi)$, $y \stackrel{\text{def}}{=} \sin(\chi) \sin(\theta) \sin(\varphi)$, $z \stackrel{\text{def}}{=} \sin(\chi) \cos(\theta)$, $w \stackrel{\text{def}}{=} \cos(\theta)$ [48] (where, as usual, $\theta \in [0, \pi]$ is the polar angle, $\varphi \in [0, 2\pi]$ is the azimuthal angle, and $\chi \in (0, \pi)$ is the hyperspherical angle [49]), the spatial line element dl^2 in Eq. (B3) becomes

$$dl_{\text{RW}}^2 \stackrel{\text{def}}{=} d\chi^2 + \sin^2(\chi) [d\theta^2 + \sin^2(\theta) d\varphi^2], \quad (\text{B4})$$

with $r \stackrel{\text{def}}{=} (x^2 + y^2 + z^2)^{1/2} = \sin(\chi)$. The quantity dl_{RW}^2 in Eq. (B4) coincides with ds_{Bures}^2 in Eq. (B1) and represents the metric of a three-sphere S^3 of unit radius. The three-sphere S^3 can be visualized as embedded in a four-dimensional Euclidean space and specified by the condition $x^2 + y^2 + z^2 + w^2 = 1$. Interestingly, just as excursions off the three sphere S^3 are physically meaningless and forbidden in general relativity [48], quantum systems in single-qubit mixed states cannot escape from the inside of the Bloch sphere. Finally, for a discussion on the measurement of lengths in curved space-time, we refer for completeness to Refs. [50–53].